

# Dynamical quark loop light-by-light contribution to muon $g-2$ within the nonlocal chiral quark model

A. E. Dorokhov<sup>1,2,a</sup>, A. E. Radzhabov<sup>3,b</sup>, A. S. Zhevlakov<sup>3,4,c</sup>

<sup>1</sup> Bogoliubov Laboratory of Theoretical Physics, JINR, Dubna 141980, Russia

<sup>2</sup> N.N. Bogoliubov Institute of Theoretical Problems of Microworld, M.V. Lomonosov Moscow State University, Moscow 119991, Russia

<sup>3</sup> Institute for System Dynamics and Control Theory SB RAS, Irkutsk 664033, Russia

<sup>4</sup> Department of Physics, Tomsk State University, Lenin ave. 36, Tomsk 634050, Russia

Received: 28 April 2015 / Accepted: 23 July 2015 / Published online: 9 September 2015  
© The Author(s) 2015. This article is published with open access at Springerlink.com

**Abstract** The hadronic corrections to the muon anomalous magnetic moment  $a_\mu$ , due to the gauge-invariant set of diagrams with dynamical quark loop light-by-light scattering insertions, are calculated in the framework of the nonlocal chiral quark model. These results complete calculations of all hadronic light-by-light scattering contributions to  $a_\mu$  in the leading order in the  $1/N_c$  expansion. The result for the quark loop contribution is  $a_\mu^{\text{HLbL,Loop}} = (11.0 \pm 0.9) \times 10^{-10}$ , and the total result is  $a_\mu^{\text{HLbL,N}\chi\text{QM}} = (16.8 \pm 1.2) \times 10^{-10}$ .

## 1 Introduction

Experimental and theoretical research on lepton anomalous magnetic moments has a long and prominent history.<sup>1</sup> The most recent and precise measurements of the muon anomalous magnetic moment  $a_\mu$  were published in 2006 by the E821 collaboration at the Brookhaven National Laboratory [5]. The combined result, based on nearly equal samples of positive and negative muons, is

$$a_\mu^{\text{BNL}} = 116\,592\,08.0 (6.3) \times 10^{-10} \quad [0.54 \text{ ppm}]. \quad (1)$$

Later on, this value was corrected [6, 7] for a small shift in the ratio of the magnetic moments of the muon and the proton as

$$a_\mu^{\text{BNL,CODATA}} = 116\,592\,09.1 (6.3) \times 10^{-10}. \quad (2)$$

<sup>1</sup> For comprehensive reviews see [1–4].

<sup>a</sup> e-mail: dorokhov@theor.jinr.ru

<sup>b</sup> e-mail: aradzh@icc.ru

<sup>c</sup> e-mail: zhevlakov@phys.tsu.ru

This exciting result is still limited by the statistical errors, and proposals to measure  $a_\mu$  with a fourfold improvement in accuracy were suggested at Fermilab (USA) [8] and J-PARC (Japan) [9]. These plans are very important in view of a very accurate prediction of  $a_\mu$  within the standard model (SM). The dominant contribution in the SM comes from QED,

$$a_\mu^{\text{QED}} = 116\,584\,71.8951(80) \times 10^{-10} \quad [10]. \quad (3)$$

Other contributions are due to the electroweak corrections [11, 12],

$$a_\mu^{\text{EW}} = 15.36(0.1) \times 10^{-10} \quad [12], \quad (4)$$

the hadron vacuum polarization (HVP) contributions in the leading, next-to-leading and next-next-to-leading order [13–15],

$$a_\mu^{\text{HVP,LO}} = 694.91(3.72)(2.10) \times 10^{-10} \quad [13], \quad (5)$$

$$a_\mu^{\text{HVP,NLO}} = -9.84(0.06)(0.04) \times 10^{-10} \quad [13], \quad (6)$$

$$a_\mu^{\text{HVP,NNLO}} = 1.24(0.01) \times 10^{-10} \quad [14], \quad (7)$$

and the hadronic light-by-light (HLbL) scattering contribution (as estimated in [16]),

$$a_\mu^{\text{HLbL}} = 10.5(2.6) \times 10^{-10}. \quad (8)$$

As a result, the total value for the SM contribution, if we take (8) for HLbL, is

$$a_\mu^{\text{SM}} = 116\,591\,84.1 (5.0) \times 10^{-10}. \quad (9)$$

From the comparison of (2) with (9) it follows that there is a 3.11 standard deviation between theory and experiment. This might be evidence for the existence of new interactions,

and it stringently constrains the parametric space of hypothetical interactions extending the SM.<sup>2</sup>

From the above it is clear that the main source of theoretical uncertainties comes from the hadronic contributions. The HVP contribution  $a_\mu^{\text{HVP,LO}}$ , using analyticity and unitarity, can be expressed as a convolution integral over the invariant mass of a known kinematical factor and the total  $e^+e^- \rightarrow \gamma^* \rightarrow \text{hadrons}$  cross section [18–21]. Then the corresponding error in  $a_\mu^{\text{HVP,LO}}$  essentially depends on the accuracy in the measurement of the cross section [13,15]. In the near future it is expected that new and precise measurements from CMD3 and SND at VEPP-2000 in Novosibirsk, BES III in Beijing, and KLOE-2 at DAFNE in Frascati will allow one to significantly increase the accuracy of the predictions for  $a_\mu^{\text{HVP,LO}}$ .

On the other hand, the HLbL contribution  $a_\mu^{\text{HLbL}}$  cannot be calculated from first principles or (unlike to HVP) be directly extracted from phenomenological considerations. Instead, it has to be evaluated using various QCD inspired hadronic models that correctly reproduce basic low- and high-energy properties of the strong interaction. Nevertheless, as will be discussed below, it is important for model calculations that phenomenological information and well-established theoretical principles should significantly reduce the number of model assumptions and the allowable space of model parameters.

Different approaches to the calculation of the contributions from the HLbL scattering process to  $a_\mu^{\text{HLbL}}$  have been suggested. These approaches can be classified into several types. The first one consists of various extended versions of the vector meson dominance model (VMD) supplemented by the ideas of the chiral effective theory, such as the hidden local symmetry model (HLS) [22,23], the lowest meson dominance (LMD) [24–26], and the (resonance) chiral perturbative theory ((R) $\chi$ PT) [27–29]. The second type of approaches is based on the consideration of effective models of QCD that use the dynamical quarks as effective degrees of freedom. The rest include different versions of the (extended) Nambu–Jona-Lasinio model (E)NJL [30–32], the constituent quark models with local interaction (CQM) [33–37], the models based on nonperturbative quark–gluon dynamics, like the nonlocal chiral quark model (N $\chi$ QM) [38–44], the Dyson–Schwinger model [45,46] (DS), or holographic models (HM) [47,48]. More recently, there have been attempts to estimate  $a_\mu^{\text{HLbL}}$  within the dispersive approach (DA) [49,50] and the so-called rational approximation (RA) approach [51,52].

The aim of this work is to complete calculations of the contributions leading in  $1/N_c$  HLbL within the N $\chi$ QM started in [43,44] and to compare the result with (8). Namely, in

previous works we made detailed calculations of hadronic contributions due to the exchange diagrams in the channels of light pseudoscalar and scalar mesons. In the present work, the detailed calculation of the light quark loop contribution is given.<sup>3</sup>

## 2 Light-by-light contribution to $a_\mu$ in the general case

We start from some general consideration of the connection between the muon AMM and the light-by-light (LbL) scattering polarization tensor. The muon AMM for the LbL contribution can be extracted by using the projection [53]

$$a_\mu^{\text{LbL}} = \frac{1}{48m_\mu} \text{Tr}((\hat{p} + m_\mu)[\gamma^\rho, \gamma^\sigma](\hat{p} + m_\mu)\Pi_{\rho\sigma}(p, p)), \tag{10}$$

where

$$\begin{aligned} \Pi_{\rho\sigma}(p', p) = e^6 \int \frac{d^4q_1}{(2\pi)^4} \int \frac{d^4q_2}{(2\pi)^4} \frac{1}{q_2^2(q_1 + q_2)^2(q_1 + k)^2} \\ \times \gamma^\mu \frac{\hat{p}' - \hat{q}_2 + m_\mu}{(p' - q_2)^2 - m_\mu^2} \gamma^\nu \frac{\hat{p} + \hat{q}_1 + m_\mu}{(p + q_1)^2 - m_\mu^2} \gamma^\lambda \\ \times \frac{\partial}{\partial k_\rho} \Pi_{\mu\nu\lambda\sigma}(q_2, -(q_1 + q_2), k + q_1, -k), \end{aligned} \tag{11}$$

where  $m_\mu$  is the muon mass,  $k_\mu = (p' - p)_\mu$ , and it is necessary to make the static limit  $k_\mu \rightarrow 0$  after differentiation. Let us introduce the notation

$$\begin{aligned} \frac{\partial}{\partial k_\rho} \Pi_{\mu\nu\lambda\sigma}(q_2, -(q_1 + q_2), k + q_1, -k) \\ = \Pi_{\rho\mu\nu\lambda\sigma}(q_2, -(q_1 + q_2), q_1) + O(k) \end{aligned} \tag{12}$$

for the derivative of the four-rank polarization tensor,<sup>4</sup> and rewrite Eqs. (10) and (11) in the form ( $q_3 \equiv q_1 + q_2$ )

$$\begin{aligned} a_\mu^{\text{LbL}} = \frac{e^6}{48m_\mu} \int \frac{d^4q_1}{(2\pi)^4} \int \frac{d^4q_2}{(2\pi)^4} \\ \times \frac{\Pi_{\rho\mu\nu\lambda\sigma}(q_2, -q_3, q_1) T^{\rho\mu\nu\lambda\sigma}(q_1, q_2, p)}{q_1^2 q_2^2 q_3^2 ((p + q_1)^2 - m_\mu^2) ((p - q_2)^2 - m_\mu^2)}, \end{aligned} \tag{13}$$

<sup>3</sup> Preliminary results of this work were announced in [3].

<sup>4</sup> First, note that the tensor  $\Pi_{\mu\nu\lambda\sigma}$  can be of any nature (QED, hadronic, etc.). Another note concerns the important result expressing the tensor  $\Pi_{\rho\mu\nu\lambda\sigma}$  in the explicitly gauge-invariant form that was obtained in [54, 55].

<sup>2</sup> In this regard we would like to mention the work [17], where a public code for computing new physics contributions to  $a_\mu$  applicable to any particle physics models is developed.

where the tensor  $T^{\rho\mu\nu\lambda\sigma}$  is the Dirac trace

$$T^{\rho\mu\nu\lambda\sigma}(q_1, q_2, p) = \text{Tr}((\hat{p} + m_\mu)[\gamma^\rho, \gamma^\sigma](\hat{p} + m_\mu) \times \gamma^\mu(\hat{p} - \hat{q}_2 + m_\mu)\gamma^\nu(\hat{p} + \hat{q}_1 + m_\mu)\gamma^\lambda).$$

Taking the Dirac trace, the tensor  $T^{\rho\mu\nu\lambda\sigma}$  becomes a polynomial in the momenta  $p, q_1, q_2$ .

After that, it is convenient to convert all momenta into the Euclidean space, and we will use the capital letters  $P, Q_1, Q_2$  for the corresponding counterparts of the Minkowskian vectors  $p, q_1, q_2$ , e.g.  $P^2 = -p^2 = -m_\mu^2, Q_1^2 = -q_1^2, Q_2^2 = -q_2^2$ . Then Eq. (13) becomes

$$a_\mu^{\text{LbL}} = \frac{e^6}{48m_\mu} \int \frac{d^4_E Q_1}{(2\pi)^4} \int \frac{d^4_E Q_2}{(2\pi)^4} \frac{1}{Q_1^2 Q_2^2 Q_3^2} \frac{T^{\rho\mu\nu\lambda\sigma} \Pi_{\rho\mu\nu\lambda\sigma}}{D_1 D_2},$$

$$D_1 = (P + Q_1)^2 + m_\mu^2 = 2(P \cdot Q_1) + Q_1^2, \tag{14}$$

$$D_2 = (P - Q_2)^2 + m_\mu^2 = -2(P \cdot Q_2) + Q_2^2.$$

Since the highest order of the power of the muon momentum  $P$  in  $T^{\rho\mu\nu\lambda\sigma}$  is two<sup>5</sup> and  $\Pi_{\rho\mu\nu\lambda\sigma}$  is independent of  $P$ , the factors in the integrand of (14) can be rewritten as

$$\frac{T^{\rho\mu\nu\lambda\sigma} \Pi_{\rho\mu\nu\lambda\sigma}}{D_1 D_2} = \sum_{a=1}^6 A_a \tilde{\Pi}_a, \tag{15}$$

with the coefficients

$$A_1 = \frac{1}{D_1}, \quad A_2 = \frac{1}{D_2}, \quad A_3 = \frac{(P \cdot Q_2)}{D_1},$$

$$A_4 = \frac{(P \cdot Q_1)}{D_2}, \quad A_5 = \frac{1}{D_1 D_2}, \quad A_6 = 1, \tag{16}$$

where all  $P$  dependence is included in the  $A_a$  factors, while  $\tilde{\Pi}_a$  are  $P$  independent.

Then one can average over the direction of the muon momentum  $P$  (as was suggested in [1] for the pion-exchange contribution),

$$\int \frac{d^4_E Q_1}{(2\pi)^4} \int \frac{d^4_E Q_2}{(2\pi)^4} \frac{A_a}{Q_1^2 Q_2^2 Q_3^2} \dots$$

$$= \frac{1}{2\pi^2} \int_0^\infty dQ_1 \int_0^\infty dQ_2 \int_{-1}^1 dt \sqrt{1-t^2} \frac{Q_1 Q_2}{Q_3^2} \langle A_a \rangle \dots, \tag{17}$$

<sup>5</sup> The possible combinations with momentum  $P$  are

$$(P \cdot Q_1)^2 = (P \cdot Q_1)(D_1 - Q_1^2)/2,$$

$$(P \cdot Q_2)^2 = -(P \cdot Q_2)(D_2 - Q_2^2)/2,$$

$$(P \cdot Q_1)(P \cdot Q_2) = -(D_1 - Q_1^2)(D_2 - Q_2^2)/4,$$

$$(P \cdot Q_1) = (D_1 - Q_1^2)/2, \quad (P \cdot Q_2) = -(D_2 - Q_2^2)/2.$$

where the radial variables of integration  $Q_1 \equiv |Q_1|$  and  $Q_2 \equiv |Q_2|$  and the angular variable  $t = (Q_1 \cdot Q_2) / (|Q_1||Q_2|)$  are introduced.

The averaged  $A_a$  factors are [1]

$$\langle A \rangle_1 = \left\langle \frac{1}{D_1} \right\rangle = \frac{R_1 - 1}{2m_\mu^2}, \quad \langle A \rangle_2 = \left\langle \frac{1}{D_2} \right\rangle = \frac{R_2 - 1}{2m_\mu^2},$$

$$\langle A \rangle_3 = \left\langle \frac{(P \cdot Q_2)}{D_1} \right\rangle = +(Q_1 \cdot Q_2) \frac{(1 - R_1)^2}{8m_\mu^2}, \tag{18}$$

$$\langle A \rangle_4 = \left\langle \frac{(P \cdot Q_1)}{D_2} \right\rangle = -(Q_1 \cdot Q_2) \frac{(1 - R_2)^2}{8m_\mu^2},$$

$$\langle A \rangle_5 = \left\langle \frac{1}{D_1 D_2} \right\rangle = \frac{1}{m_\mu^2 Q_1 Q_2 x} \arctan \left[ \frac{zx}{1 - zt} \right],$$

$$\langle A \rangle_6 = \langle 1 \rangle = 1,$$

with

$$x = \sqrt{1 - t^2}, \quad R_i = \sqrt{1 + \frac{4m_\mu^2}{Q_i^2}} \quad (i = 1, 2), \tag{19}$$

$$z = \frac{Q_1 Q_2}{4m_\mu^2} (1 - R_1)(1 - R_2).$$

After averaging the LbL contribution can be represented in the form

$$a_\mu^{\text{LbL}} = \int_0^\infty dQ_1 \int_0^\infty dQ_2 \rho^{\text{LbL}}(Q_1, Q_2), \tag{20}$$

with the density  $\rho^{\text{LbL}}(Q_1, Q_2)$  being defined as

$$\rho^{\text{LbL}}(Q_1, Q_2) = \frac{Q_1 Q_2}{2\pi^2} \sum_{a=1}^6 \int_{-1}^1 dt \frac{\sqrt{1-t^2}}{Q_3^2} \langle A_a \rangle \tilde{\Pi}_a. \tag{21}$$

Thus, the number of momentum integrations in the original expression for (10) is reduced from eight to three. The transformations leading from (10) to (20) are of a general nature, independent of the theoretical (model) assumptions on the form of the polarization tensors  $\tilde{\Pi}_a$ . In particular, this 3D-representation is common for all hadronic LbL contributions: the pseudoscalar meson-exchange contributions [1,43], the scalar meson-exchange contributions [44], and the quark loop contributions discussed in the present work. The next problem to be elaborated is the calculation of the density  $\rho^{\text{HLbL}}(Q_1, Q_2)$  in the framework of the model.

### 3 Hadronic light-by-light contribution to $a_\mu$ within $N\chi$ QM

Let us briefly review the basic facts about the  $N\chi$ QM.<sup>6</sup> The Lagrangian of the  $SU(3)$  nonlocal chiral quark model with the  $SU(3) \times SU(3)$  symmetry has the form

$$\mathcal{L} = \bar{q}(x)(i\hat{\partial} - m_c)q(x) + \frac{G}{2}[J_S^a(x)J_S^a(x) + J_{PS}^a(x)J_{PS}^a(x)] - \frac{H}{4}T_{abc}[J_S^a(x)J_S^b(x)J_S^c(x) - 3J_S^a(x)J_{PS}^b(x)J_{PS}^c(x)], \tag{22}$$

where  $q(x)$  are the quark fields,  $m_c$  ( $m_{c,u} = m_{c,d} \neq m_{c,s}$ ) is the diagonal matrix of the quark current masses, and  $G$  and  $H$  are the four- and six-quark coupling constants. The nonlocal structure of the model is introduced via the nonlocal quark currents

$$J_M^a(x) = \int d^4x_1 d^4x_2 F(x_1, x_2) \bar{q}(x - x_1) \Gamma_M^a q(x + x_2), \tag{23}$$

where  $M = S$  for the scalar and  $M = PS$  for the pseudoscalar channels,  $\Gamma_S^a = \lambda^a$ ,  $\Gamma_{PS}^a = i\gamma^5 \lambda^a$ , and  $F(x_1, x_2)$  is the form factor with the nonlocality parameter  $\Lambda$  reflecting the nonlocal properties of the QCD vacuum. The  $SU(2)$  version of the  $N\chi$ QM with  $SU(2) \times SU(2)$  symmetry is obtained by setting  $H$  to zero and taking only scalar–isoscalar and pseudoscalar–isovector currents.

Within the  $N\chi$ QM, the standard mechanism for spontaneous breaking of chiral symmetry occurs, which is typical for the Nambu–Jona-Lasinio type models with the chiral symmetric four-fermion interaction (local or nonlocal). Due to this interaction the massless quark becomes massive, and in the hadron spectrum the gap between the massless (in the chiral limit) Nambu–Goldstone pion and the massive scalar meson appears. This feature is common for the models used for the calculation of the hadronic contributions to the muon  $g-2$ : the extended NJL model [30–32], the constituent chiral quark model [37], the Dyson–Schwinger model [45,46], the nonlocal chiral quark model [38–44]. In the nonlocal models the dynamically generated quark mass becomes momentum dependent and the inverse dynamical quark propagator takes the form

$$S^{-1}(k) = \hat{k} - m(k^2) \tag{24}$$

where  $m(k^2) = m_c + m_D F(k^2, k^2)$  is the dynamical quark mass obtained by solving the Dyson–Schwinger equation. The significant feature of the nonlocal models [38–40] is that

<sup>6</sup> More detailed information as regards the model is contained in our previous works [42,44].

they correctly interpolate between the low-energy region (and are consistent with the low-energy theorems) and the high-energy region (where they are consistent with OPE). The basic fact is that the momentum-dependent dynamical quark mass, that is, the constituent quark mass  $m(0) = m_c + m_D$  at low virtualities, becomes the current quark mass  $m_c$  at large virtualities. This is in contrast to the local models, where the quark mass is the constituent one at any virtuality.

For numerical estimates two versions of the form factor (in momentum space) are used: the Gaussian form factor

$$F_G(k_E^2, k_E^2) = \exp(-2k_E^2/\Lambda^2), \tag{25}$$

and the Lorentzian form factor

$$F_L(k_E^2, k_E^2) = \frac{1}{(1 + k_E^2/\Lambda^2)^2}. \tag{26}$$

The second version is used in order to test the stability of the results to the nonlocality shape.

Next, it is necessary to introduce in the nonlocal chiral Lagrangian (22) the gauge-invariant interaction with an external photon field  $A_\mu(z)$ . This can be done through the introduction of the path-ordered Schwinger phase factor for the quark field,

$$q(y) \rightarrow Q(x, y) = \mathcal{P} \exp \left\{ i \int_x^y dz^\mu A_\mu(z) \right\} q(y). \tag{27}$$

Then, apart from the kinetic term, the additional, nonlocal terms in the interaction of quarks with the gauge field are generated via the substitution

$$J_M^a(x) \rightarrow J_M^a(x) = \int d^4x_1 d^4x_2 f(x_1) f(x_2) \times \bar{Q}(x - x_1, x) \Gamma_M^a Q(x, x + x_2), \tag{28}$$

inducing the quark–antiquark– $n$ -photon vertices. In order to obtain the explicit form of these vertices, it is necessary to fix the rules for the contour integral in the phase factor. The scheme, based on the rules that the derivative of the contour integral does not depend on the path shape,

$$\frac{\partial}{\partial y^\mu} \int_x^y dz^\nu F_\nu(z) = F_\mu(y), \quad \delta^{(4)}(x - y) \int_x^y dz^\nu F_\nu(z) = 0,$$

was suggested in [56] and applied to nonlocal models in [57]. For our purpose, we need to consider the quark–antiquark vertices with one, two, three, and four photons (Fig. 1). The first two types of vertices were derived in [57], the vertex with three photons was obtained in [58], and the quark–four-photon vertex is given in the present work. Their explicit form and the definition for the finite-difference derivatives

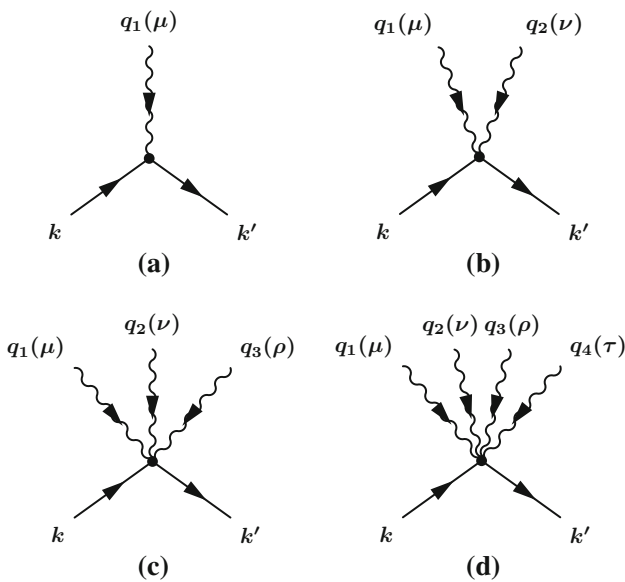


**Fig. 1** The quark–photon vertex  $\Gamma_\mu^{(1)}(q)$ , the quark–two-photon vertex  $\Gamma_{\mu\nu}^{(2)}(q_1, q_2)$ , the quark–three-photon vertex  $\Gamma_{\mu\nu\rho}^{(3)}(q_1, q_2, q_3)$ , and the quark–four-photon vertex  $\Gamma_{\mu\nu\rho\tau}^{(4)}(q_1, q_2, q_3, q_4)$

$m^{(n)}(k, k')$  are presented in the appendix. The simplest quark–photon vertex has the usual local part as well as the nonlocal piece in terms of the first finite-difference derivative  $m^{(1)}(k, k')$ ,

$$\Gamma_\mu^{(1)}(q_1) = \gamma_\mu + \Delta\Gamma_\mu^{(1)}(q_1), \tag{29}$$

$$\Delta\Gamma_\mu^{(1)}(q_1) = -(k + k')_\mu m^{(1)}(k, k'), \tag{30}$$

while the quark–antiquark vertices with more than one photon insertion are purely nonlocal (see the appendix).

We have to remind the reader that in the models with the chiral symmetric four-quark interaction (nonlocal or local NJL type) the Goldstone particles and other mesons appear as the poles in the quark–antiquark scattering matrix due to the summation of an infinite number of diagrams [22, 23, 30–32, 37, 42, 43, 45, 46]. In these diagrams, the quark and antiquark interact via the four-quark interaction. On the other hand, in the box diagram (Fig. 2), the quark and antiquark do not interact and thus they are separated from the set of diagrams producing mesons as bound states. It means, in particular, that

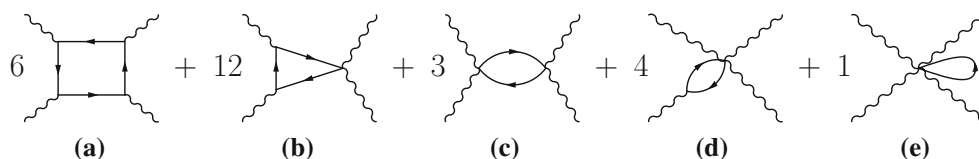


**Fig. 2** The box diagram and the diagrams with nonlocal multi-photon interaction vertices represent the gauge-invariant set of diagrams contributing to the polarization tensor  $\Pi_{\mu\nu\lambda\rho}(q_1, q_2, q_3, q_4)$ . The numbers in front of the diagrams are the combinatoric factors

in these approaches there are no double-counting effects. On the other hand in the framework NJL model it was shown that these two types of contributions, e.g. box and bound state one, are necessary for the correct description of such processes as pion polarizability [59] or  $\pi\pi$ -scattering [60] and omitting one of these contributions will lead to large breaking of the chiral symmetry.

We may add that, from the quark–hadron duality arguments, the quark loop (as for the two-point correlator as well for the four-point correlator) represents the contribution of the continuum of excited hadronic states. In the language of the spectral densities, the model calculations correspond to the model of the spectral density saturated by the lowest hadronic resonance plus the excited hadronic state continuum. The first part is for the meson-exchange diagrams, and the latter for the quark loop. It is the quark loop (continuum) that provides the correct large photon momentum QCD asymptotics for the Adler function, three- and four-point correlators.

With the Feynman rules for the dynamical quark propagator (24) and the quark–photon vertices (29), (A.2), (A.3), and (A.4), the gauge-invariant set of diagrams describing the polarization tensor  $\Pi_{\mu\nu\lambda\sigma}(q_2, -(q_1 + q_2), k + q_1, -k)$  due to the dynamical quark loop contribution is given in Fig. 2.

### 4 The results

For the numerical estimates, the SU(2)- and SU(3)-versions of the  $N_\chi$ QM model are used. In order to check the model dependence of the final results, we also perform calculations for different sets of model parameters.

In the SU(2) model, the same scheme of fixing the model parameters as in [43, 44] is applied: fitting the parameters  $\Lambda$  and  $m_c$  by the physical values of the  $\pi^0$  mass and the  $\pi^0 \rightarrow \gamma\gamma$  decay width, and varying  $m_D$  in the region 150–400 MeV. For an estimation of  $a_\mu^{\text{HLbL}}$  and its error, we use the region for  $m_D$  from 200 to 350 MeV.

For the SU(3) version of the model, it is necessary to fix two more parameters: the current and dynamical masses of the strange quark. We suggest to fix them by fitting the  $K^0$  mass and obtaining more or less reasonable values for the  $\eta$  meson mass and the  $\eta \rightarrow \gamma\gamma$  decay width. The main problem

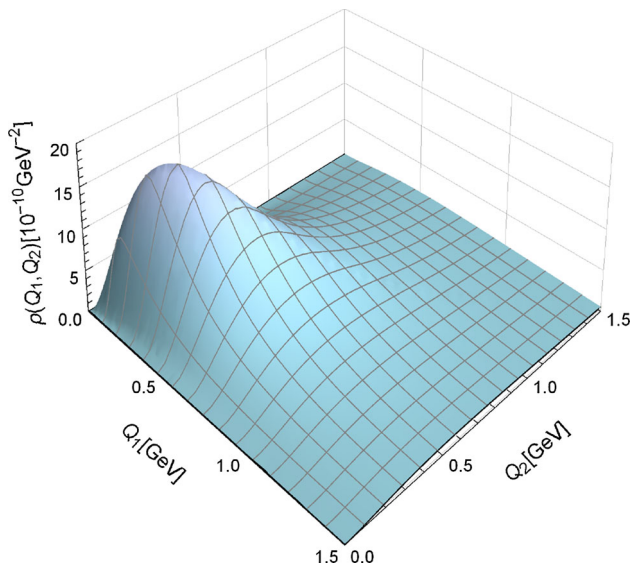


**Fig. 3** The 3D density  $\rho(Q_1, Q_2)$  defined in Eqs. (20) and (21)

here is that the lowest value for the nonstrange dynamical mass  $m_D$  is 240 MeV, because at lower  $m_D$  the  $\eta$  meson becomes unstable within the model approach.

Additionally, in order to show that the different schemes of parameter fixing will lead to similar results for  $a_\mu^{\text{HLbL}}$ , we calculate this quantity for the model (22) with parameters taken from [61] for the Gaussian ( $G_I$ – $G_{IV}$ ) and the Lorentzian ( $L_I$ – $L_{IV}$ ) nonlocal form factors. The authors of [61] have used another scheme of parameter fixing. Namely, the value of the light current quark mass is fixed (8.5 MeV for  $G_I$ – $G_{III}$ , 7.5 MeV for  $G_{IV}$ , 4.0 MeV for  $L_I$ – $G_{III}$ , and 3.5 MeV for  $L_{IV}$ ). The other parameters are fitted in order to reproduce the values of the pion and kaon masses, the pion decay constant  $f_\pi$ , and, alternatively, the  $\eta'$  mass for sets  $G_I, G_{IV}, L_I, L_{IV}$  or the  $\eta' \rightarrow \gamma\gamma$  decay width for the sets  $G_{II}, G_{III}, L_{II}, L_{III}$ .

The important result, independent of the parameterizations, is the behavior of the density  $\rho^{\text{HLbL}}(Q_1, Q_2)$ , shown in Fig. 3. One can see that  $\rho^{\text{HLbL}}(Q_1, Q_2)$  is zero at the edges ( $Q_1 = 0$  or  $Q_2 = 0$ ) and is concentrated in the low-energy region<sup>7</sup> ( $Q_1 \approx Q_2 \approx 300$  MeV), providing the dominant contribution to  $a_\mu^{\text{HLbL}}$ . This behavior at the edges appears to be due to cancellations of contributions from different diagrams of Fig. 2.

In Fig. 4, the slice of  $\rho^{\text{HLbL}}(Q_1, Q_2)$  in the diagonal direction  $Q_2 = Q_1$  is presented together with the partial contributions from the diagrams of different topology. One can see that the  $\rho^{\text{HLbL}}(0, 0) = 0$  is due to a nontrivial cancellation of different diagrams of Fig. 2. This important result is a consequence of gauge invariance and the spontaneous viola-

<sup>7</sup> One should point out that the density for the mesonic exchanges shows a similar behavior.

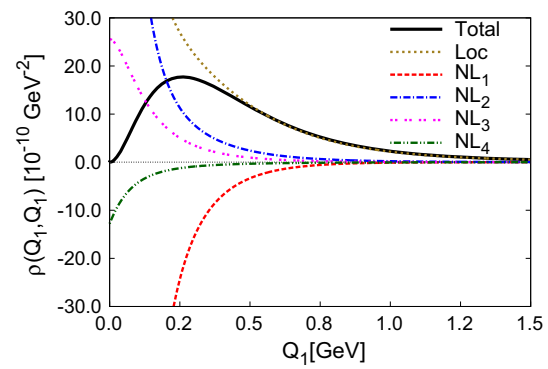


**Fig. 4** The 2D slice of the density  $\rho(Q_1, Q_2)$  at  $Q_2 = Q_1$ . Different curves correspond to the contributions of topologically different sets of diagrams drawn in Fig. 2. The contribution of the box diagram with the local vertices, Fig. 2a, is the dot (olive) line (Loc); the box diagram, Fig. 2a, with the nonlocal parts of the vertices is the dash (red) line (NL<sub>1</sub>); the triangle, Fig. 2b, and loop, Fig. 2c, diagrams with the two-photon vertices is the dash-dot (blue) line (NL<sub>2</sub>); the loop with the three-photon vertex, Fig. 2d, is the dot-dot (magenta) line (NL<sub>3</sub>); the loop with the four-photon vertex, Fig. 2e, is the dash-dot-dot (green) line (NL<sub>4</sub>); the sum of all contributions (total) is the solid (black) line. At zero all contributions are finite

tion of the chiral symmetry, and it represents the low-energy theorem analogous to the theorem for the Adler function at zero momentum. Another interesting feature is that the large  $Q_1, Q_2$  behavior is dominated by the box diagram with local vertices and quark propagators with momentum-independent masses in accordance with perturbative theory. All this is a very important characteristic of the N $\chi$ QM, interpolating the well-known results of the  $\chi$ PT at low momenta and the operator product expansion at large momenta. Earlier, similar results were obtained for the two-point [38,39] and three-point [40] correlators.

The numerical results for the value of  $a_\mu^{\text{HLbL}}$  are given in the Table 1 and presented in Fig. 5 for the SU(2) and SU(3) models together with the result of C $\chi$ QM [37] and DSE [45,46] calculations. The estimates for the partial contributions to  $a_\mu^{\text{HLbL}}$  (in  $10^{-10}$ ) are the  $\pi^0$  contribution, 5.01(0.37) [43], the sum of the contributions from  $\pi^0, \eta,$  and  $\eta'$  mesons, 5.85(0.87) [43], the scalar  $\sigma, a_0(980),$  and  $f_0(980)$  mesons contribution, 0.34(0.48) [3,44], and the quark loop contribution, 11.0(0.9) [3]. In all cases we estimate the absolute value of the result and its error by calculating  $a_\mu^{\text{HLbL}, N\chi\text{QM}}$  for the space of model parameters fixed by the above mentioned observables, except one, varying  $m_D$ . Because in all cases the resulting curves (Fig. 5) are quite smooth, it gives to us credit to point out rather small model errors ( $\leq 10\%$ ) for the intermediate and final results. Thus our claim is that the total contribution obtained in the leading order in the  $1/N_c$  expansion within the nonlocal chiral quark model is (see also [3]).

**Table 1** The contribution to the muon AMM  $a_{\mu}^{\text{LBL}}$  for different sets of model parameters. The model parameters  $G_{I-IV}$  and  $L_{I-IV}$  are taken from [61]. The difference between  $a_{\mu}^{\text{LBL}}$  for the set of model parameters with the same  $u$  quark mass in SU(2) and SU(3) models is due to the mixing of the  $\sigma$  meson with the  $f_0$  meson in the SU(3) case. In order to extrapolate the SU(3)-result to lower quark masses, we find that the maximal value of the difference between the total SU(2)- and SU(3)-results is 0.77. We add this number to the value of the SU(2)-result at 200 MeV

No.	Model parameters										$a_{\mu}^{\text{LBL}}$ in $10^{-10}$						
	$m_{d,u}$ (MeV)	$m_{c,u}$ (MeV)	$m_{d,s}$ (MeV)	$m_{c,s}$ (MeV)	$\Lambda$ (MeV)	Total SU(3)	Total SU(2)	$u + d$ quark loop	$s$ quark loop	$\pi^0 + \sigma$	$\eta + \eta' + a_0 + f_0$						
1	150	0.33			6786.6		21.74	16.95		4.79							
2	160	0.59			4890.7		20.49	15.38		5.11							
3	170	0.93			3768.9		19.45	14.10		5.35							
4	180	1.33			3049.2		18.60	13.10		5.50							
5	190	1.78			2557.6		17.89	12.29		5.60							
6	200	2.27			2204.9		17.30	11.67		5.64							
7	210	2.79			1941.5		16.82	11.18		5.64							
8	220	3.34			1738.2		16.42	10.80		5.62							
9	230	3.90			1577.1		16.09	10.52		5.58							
10	240	4.47			1446.3		15.83	10.31		5.52							
11	240	4.47	339.5	133.7	1446.3	16.53	15.89	10.31	0.234	5.58	0.404						
12	250	5.06			1338.2		15.61	10.16		5.46							
13	250	5.06	347.1	148.4	1338.2	16.21	15.64	10.16	0.229	5.49	0.337						
14	260	5.65			1247.2		15.45	10.05		5.39							
15	270	6.25			1169.6		15.31	9.99		5.33							
16	280	6.86			1102.5		15.23	9.97		5.26							
17	280	6.86	387.4	193.4	1102.5	15.91	15.22	9.97	0.209	5.25	0.480						
18	290	7.48			1043.9		15.14	9.94		5.19							
19	300	8.09			992.2		15.08	9.96		5.12							
20	305	8.41	413.7	231.9	968.6	15.78	15.05	9.97	0.193	5.08	0.543						
21	310	8.72			946.2		15.04	9.98		5.06							
22	320	9.35			904.9		15.02	10.02		5.00							
23	320	9.35	428	255.7	904.9	15.78	15.02	10.03	0.182	4.99	0.577						
24	330	9.99			867.7		15.01	10.08		4.94							
25	340	10.63			833.8		15.02	10.14		4.88							
26	350	11.29			802.8		15.03	10.21		4.82							
27	350	11.29	451.2	305.9	802.8	15.80	15.05	10.21	0.159	4.84	0.592						
28	360	11.95			774.4		15.07	10.30		4.77							
29	370	12.62			748.1		15.10	10.38		4.72							
30	380	13.30			723.8		15.14	10.47		4.67							

**Table 1** continued

No.	Model parameters										$a_{\mu}^{\text{HLbL}}$ in $10^{-10}$				
	$m_{d,u}$ (MeV)	$m_{c,u}$ (MeV)	$m_{d,s}$ (MeV)	$m_{c,s}$ (MeV)	$\Lambda$ (MeV)	Total SU(3)	Total SU(2)	$u + d$ quark loop	$s$ quark loop	$\pi^0 + \sigma$	$\eta + \eta' + a_0 + f_0$				
31	390	13.99			701.1	15.19	10.56			4.63					
32	400	14.69			679.8	15.24	10.65			4.58					
G <sub>I</sub>	304.5	8.50	427	223	1002.7	15.67	9.71	0.192		4.95	0.810				
G <sub>II</sub>	304.5	8.50	439	223	1002.7	15.93	9.71	0.190		4.95	1.070				
G <sub>III</sub>	304.5	8.50	422	223	1002.7	15.57	9.71	0.193		4.95	0.707				
G <sub>IV</sub>	287.5	7.50	408	199	1086.1	15.75	9.75	0.202		5.06	0.738				
L <sub>I</sub>	295	4.00	450	112	1013	15.58	9.61	0.241		5.23	0.503				
L <sub>II</sub>	295	4.00	505	110	1013	16.37	9.61	0.222		5.23	1.311				
L <sub>III</sub>	296	4.00	457	112	1013	15.61	9.57	0.238		5.22	0.578				
L <sub>IV</sub>	277.5	3.50	418	100	1110	15.76	9.74	0.251		5.33	0.435				

$$a_{\mu}^{\text{HLbL}, N\chi\text{QM}} = 16.8(1.25) \times 10^{-10}. \tag{31}$$

This value accounts for the spread of the results depending on a reasonable variation of the model parameters and sensitivity to the different choices of the nonlocality shapes. Note that, as was emphasized in [37], the results of these kinds of calculations do not include the “systematic error” of the models.

Comparing with other model calculations, we conclude that our results are quite close to the recent results obtained in [37,45,46].<sup>8</sup> It is not accidental. Closest to our model is the Dyson–Schwinger model used in [45,46]. The specific feature of both models is that the kernel of the nonlocal interaction is motivated by QCD. In [45,46] the kernel of the interaction is generated by the nonperturbative gluon exchanges. In the  $N\chi\text{QM}$  the form of the kernel is motivated by the instanton vacuum models. The other difference between the  $N\chi\text{QM}$  and [45,46] is that, in a sense, the  $N\chi\text{QM}$  has a minimal structure (with respect to the number of Lorentz structures for vertices, etc.). Nevertheless, the predictions of the  $N\chi\text{QM}$  for the different contributions to the muon  $g-2$  are in agreement with [45,46] within 10 %.

The constituent chiral quark model used in [37] corresponds to the local limit of the  $N\chi\text{QM}$ . This limit is achieved when the nonlocality parameter  $\Lambda$  goes to infinity, which means that the nonlocal form factors become constants:  $F(k^2, p^2) \rightarrow 1$ . Taking this limit the  $N\chi\text{QM}$  becomes one-parametric (only  $M_q$ ) and we reproduce the  $M_q$  dependence of the quark box contribution to  $a_{\mu}^{\text{HLbL}}$  shown in Fig. 13 of [37]. What is more interesting and important is that the  $M_q$  dependencies of the total contribution to  $a_{\mu}^{\text{HLbL}}$  in [37] (Fig. 14) and in the  $N\chi\text{QM}$  have the same qualitative behavior and are very close (within less than 10 %) qualitatively. This is clear from Fig. 5.

These facts are very pleasant for the phenomenology of the HLbL contributions to the muon, because it means that even starting from the models that differ in many details, the predictions are still very stable numerically.

### 5 Conclusions

In this paper, we have presented the results for the contribution of the dynamical quark loop mechanism for the light-by-light scattering to the muon anomalous magnetic moment within the nonlocal chiral quark model. In previous works [3,43,44], we calculated the corresponding contributions due to the exchange by pseudoscalar and scalar mesons. The basis

<sup>8</sup> In earlier works [22,23,30–32], the quark loop contribution was found to be one order less than in more recent calculations. In our opinion, one of the reasons is that in those models the photon–quark coupling is suppressed by the VMD form factors.



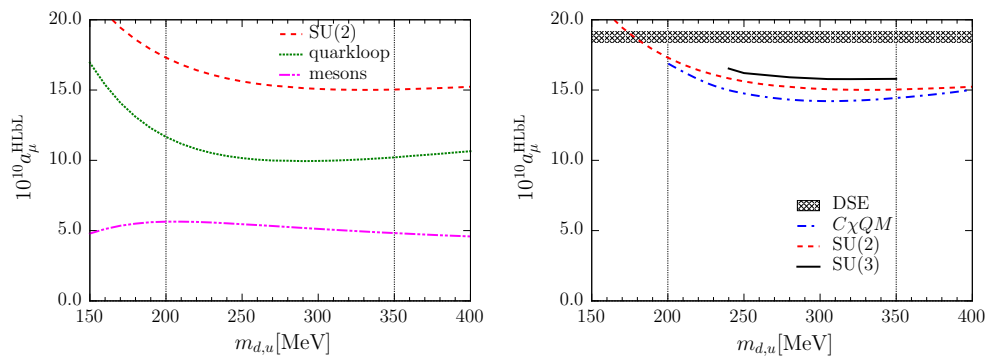


**Fig. 5** *Left* the results for  $a_\mu^{\text{HLbL}}$  in the SU(2) model: the red dashed line is the total result, the green dotted line is the quark loop contribution and the magenta dash–dot–dot line is the  $\pi + \sigma$  contribution. The thin vertical line indicates the region for the estimation of  $a_\mu^{\text{HLbL}}$  error band.

*Right* the results for  $a_\mu^{\text{HLbL}}$ : the black solid line is the SU(3)-result, the red dash line corresponds to the SU(2)-result, the blue dash–dotted line is the  $C\chi QM$  result [37], the hatched region corresponds to the DSE result [45,46]

of our model calculations is the spontaneous violation of the chiral symmetry in the model with the nonlocal four-fermion interaction and abelian gauge invariance. The first leads to the generation of the momentum-dependent dynamical quark mass, and the latter ensures the fulfillment of the Ward–Takahashi identities with respect to the quark–photon interaction.

In the present work, we derived the general expression for  $a_\mu^{\text{LbL}}$  as the three-dimensional integral in the modulus of the two photon momenta and the angle between them. The integral is the convolution of the known kinematical factors and some projections of the four-photon polarization tensor. The latter is the subject of theoretical calculations.

Since our model calculations of the hadronic contributions are basically numerical, it is more convenient to present our results in terms of the density function  $\rho^{\text{HLbL}}(Q_1, Q_2)$ . We observe some properties of this function that have a model-independent character. Firstly, at zero momenta one has  $\rho^{\text{HLbL}}(0, 0) = 0$  in spite of the fact that the partial contributions of different diagrams are nonzero in this limit. This low-energy theorem is a direct consequence of the quark–photon gauge invariance and the spontaneous violation of the chiral symmetry. Secondly, at high momenta the density is saturated by the contribution from the box diagram with the local quark–photon vertices and local quark propagators in accordance with the perturbative theory. This is a consequence of the fact that at small distances all nonperturbative nonlocal effects are washed out. Thirdly, with the model parameters chosen, the  $\rho^{\text{HLbL}}(Q_1, Q_2)$  is concentrated in the region  $Q_1 \approx Q_2 \approx 300$  MeV, which is a typical scale for light hadrons.

Summarizing the results of the present and previous works [3,43,44], we get the total hadronic contribution to  $a_\mu^{\text{HLbL}}$  within the  $N\chi QM$  in the leading order in the  $1/N_c$  expansion. The total result is given in Eq. (31). To estimate the uncertainty of this result, we vary some of the model parameters in a physically reasonable interval and also study the sensi-

tivity of the result with respect to different model parameterizations. In this sense, the error in Eq. (31) is a conservative one.

If we add the result (31) to all other known contributions of the standard model to  $a_\mu$ , (3)–(7), we see that the difference between experiment (2) and theory is

$$a_\mu^{\text{BNL,CODATA}} - a_\mu^{\text{SM}} = 18.73 \times 10^{-10}, \tag{32}$$

which corresponds to  $2.43\sigma$ . If one uses the hadronic vacuum polarization contribution from the  $\tau$  hadronic decays instead of  $e^+e^-$  data,

$$a_\mu^{\text{HVP,LO-}\tau} = 701.5(4.7) \times 10^{-10} \quad [15], \tag{33}$$

the difference decreases to  $18.44 \times 10^{-10}$  ( $2.23\sigma$ ) for the case of  $a_\mu^{\text{HLbL}}$  from (8) [16] and to  $12.14 \times 10^{-10}$  ( $1.53\sigma$ ) in our model (31).

Clearly, a further reduction of both the experimental and the theoretical uncertainties is necessary. On the theoretical side, the calculation of the still badly known HLbL contributions in the next-to-leading order in the  $1/N_c$  expansion (the pion and kaon loops) and extension of the model by including heavier vector and axial-vector mesons is the next goal. The contribution of these effects and the model error induced by them are not included in the result (31). Preliminary studies [22,23,25] show that these contributions are one order smaller than the pseudoscalar exchanges and the quark loop contributions. However, the interesting point that inclusion of the vector channel can strongly suppress contribution from the quark loop due photon–vector meson exchange, which leads to the appearance in each photon vertex of an additional VMD-like factor. This was found in local NJL model [30–32] and should be carefully investigated in the nonlocal one.

Work in this direction is now in progress, and we hope to report its results in the near future.

**Acknowledgments** We thank J. Bijnens, Yu.M. Bystritskiy, A.L. Kataev, N.I. Kochelev, E.A. Kuraev, V.P. Lomov, A. Nyffeler, H.-P. Pavel, and A.A. Pivovarov for critical remarks and illuminating discussions. Numerical calculations are performed on computing cluster “Ac. V.M. Matrosov”. The work is supported by Russian Science Foundation Grant (RSCF 15-12-10009).

**Open Access** This article is distributed under the terms of the Creative Commons Attribution 4.0 International License (<http://creativecommons.org/licenses/by/4.0/>), which permits unrestricted use, distribution, and reproduction in any medium, provided you give appropriate credit to the original author(s) and the source, provide a link to the Creative Commons license, and indicate if changes were made. Funded by SCOAP<sup>3</sup>.

**Appendix: Nonlocal multi-photon vertices**

Let us introduce the finite-difference derivatives

$$f^{(1)}(a, b) = \frac{f(a+b) - f(b)}{(a+b)^2 - b^2}, \tag{A.1}$$

$$f^{(n+1)}(a, \{b_i\}, b_1, b_2) = \frac{f^{(n)}(a, \{b_i\}, b_1) - f^{(n)}(a, \{b_i\}, b_2)}{(a+b_1)^2 - (a+b_2)^2},$$

where  $n = 1, 2, \dots$ . Then the quark–antiquark vertex with the two-photon insertions (Fig. 1b) is [57]

$$\begin{aligned} \Gamma_{\mu\nu}^{(2)}(q_1, q_2) &= 2g_{\mu\nu}m^{(1)}(k, k') \\ &+ (k+k_1)_\mu(k_1+k')_\nu m^{(2)}(k, k_1, k') \\ &+ (k+k_2)_\nu(k_2+k')_\mu m^{(2)}(k, k_2, k'). \end{aligned} \tag{A.2}$$

Here and below,  $k$  is the momentum of the incoming quark,  $k'$  is the momentum of the outgoing quark,  $q_i$  are the momenta of the incoming photons, and  $k_1 = k + q_1$ ,  $k_{ij\dots k} = k + q_i + q_j + \dots + q_k$ .

The quark–three-photon vertex (Fig. 1c) is [58]

$$\begin{aligned} \Gamma_{\mu\nu\rho}^{(3)}(q_1, q_2, q_3) &= -[2g_{\mu\nu}(k_{12}+k')_\rho m^{(2)}(k, k_{12}, k') \\ &+ 2g_{\mu\nu}(k+k_3)_\rho m^{(2)}(k, k_3, k') \\ &+ (k+k_1)_\mu(k_1+k_{12})_\nu(k_{12}+k')_\rho m^{(3)}(k, k_1, k_{12}, k') \\ &+ (k+k_1)_\mu(k_{13}+k')_\nu(k_1+k_{13})_\rho m^{(3)}(k, k_1, k_{13}, k')] \\ &+ [1 \rightleftharpoons 3, \mu \rightleftharpoons \rho] + [2 \rightleftharpoons 3, \nu \rightleftharpoons \rho]. \end{aligned} \tag{A.3}$$

The quark–four-photon vertex (Fig. 1d) takes the form

$$\begin{aligned} \Gamma_{\mu\nu\rho\tau}^{(4)}(q_1, q_2, q_3, q_4) &= [+4g_{\mu\nu}g_{\tau\rho}m^{(2)}(k, k_{12}, k') \\ &+ 4g_{\mu\nu}g_{\tau\rho}m^{(2)}(k, k_{34}, k') \\ &+ 2g_{\mu\nu}(k+k_3)_\rho(k_3+k_{34})_\tau m^{(3)}(k, k_3, k_{34}, k') \\ &+ (k+k_3)_\rho(k_{123}+k')_\tau m^{(3)}(k, k_3, k_{123}, k') \\ &+ (k_{12}+k_{123})_\rho(k_{123}+k')_\tau m^{(3)}(k, k_{12}, k_{123}, k') \end{aligned}$$

$$\begin{aligned} &+ (k_{124}+k')_\rho(k_{12}+k_{124})_\tau m^{(3)}(k, k_{12}, k_{124}, k') \\ &+ (k_{124}+k')_\rho(k+k_4)_\tau m^{(3)}(k, k_4, k_{124}, k') \\ &+ (k_4+k_{34})_\rho(k+k_4)_\tau m^{(3)}(k, k_4, k_{34}, k') \\ &+ 2g_{\tau\rho}((k+k_1)_\mu(k_1+k_{12})_\nu m^{(3)}(k, k_1, k_{12}, k') \\ &+ (k+k_2)_\nu(k_2+k_{12})_\mu m^{(3)}(k, k_2, k_{12}, k') \\ &+ (k_{34}+k_{234})_\nu(k_{234}+k_{1234})_\mu m^{(3)}(k, k_{34}, k_{234}, k') \\ &+ (k_{34}+k_{134})_\mu(k_{134}+k_{1234})_\nu m^{(3)}(k, k_{34}, k_{134}, k') \\ &+ (k+k_1)_\mu(k_{134}+k_{1234})_\nu m^{(3)}(k, k_1, k_{134}, k') \\ &+ (k+k_2)_\nu(k_{234}+k_{1234})_\mu m^{(3)}(k, k_2, k_{234}, k') \\ &+ (k+k_1)_\mu(k_1+k_{12})_\nu(k_{12}+k_{123})_\rho(k_{123}+k')_\tau \\ &\times m^{(4)}(k, k_1, k_{12}, k_{123}, k') \\ &+ (k+k_1)_\mu(k_1+k_{12})_\nu(k_{124}+k_{1234})_\rho(k_{12}+k_{124})_\tau \\ &\times m^{(4)}(k, k_1, k_{12}, k_{124}, k') \\ &+ (k_2+k_{12})_\mu(k+k_2)_\nu(k_{12}+k_{123})_\rho(k_{123}+k_{1234})_\tau \\ &\times m^{(4)}(k, k_2, k_{12}, k_{123}, k') \\ &+ (k_2+k_{12})_\mu(k+k_2)_\nu(k_{124}+k_{1234})_\rho(k_{12}+k_{124})_\tau \\ &\times m^{(4)}(k, k_2, k_{12}, k_{124}, k') \\ &+ (k_{23}+k_{123})_\mu(k+k_2)_\nu(k_2+k_{23})_\rho(k_{123}+k_{1234})_\tau \\ &\times m^{(4)}(k, k_2, k_{23}, k_{123}, k') \\ &+ (k_{24}+k_{124})_\mu(k+k_2)_\nu(k_{124}+k_{1234})_\rho(k_2+k_{24})_\tau \\ &\times m^{(4)}(k, k_2, k_{24}, k_{124}, k') \\ &+ (k_{234}+k_{1234})_\mu(k+k_2)_\nu(k_{24}+k_{234})_\rho(k_2+k_{24})_\tau \\ &\times m^{(4)}(k, k_2, k_{24}, k_{234}, k') \\ &+ (k_{234}+k_{1234})_\mu(k+k_2)_\nu(k_2+k_{23})_\rho(k_{23}+k_{234})_\tau \\ &\times m^{(4)}(k, k_2, k_{23}, k_{234}, k')] \\ &+ [2 \rightleftharpoons 4, \nu \rightleftharpoons \tau] + [2 \rightleftharpoons 3, \nu \rightleftharpoons \rho]. \end{aligned} \tag{A.4}$$

**References**

1. F. Jegerlehner, A. Nyffeler, Phys. Rep. **477**, 1 (2009)
2. J.P. Miller, E. de Rafael, B.L. Roberts, D. Stuckinger, Ann. Rev. Nucl. Part. Sci. **62**, 237 (2012)
3. A.E. Dorokhov, A.E. Radzhabov, A.S. Zhevlakov, JETP Lett. **100**(2), 133 (2014)
4. M. Knecht, [arXiv:1412.1228](https://arxiv.org/abs/1412.1228) [hep-ph]
5. G.W. Bennett et al. [Muon (g-2) Collaboration], Phys. Rev. D **73**, 072003 (2006)
6. P.J. Mohr, B.N. Taylor, D.B. Newell (CODATA Recommended Values of the Fundamental Physical Constants: 2010), Rev. Mod. Phys. **84**, 1527 (2012)
7. K.A. Olive et al. [Particle Data Group Collaboration], Chin. Phys. C **38**, 090001 (2014)
8. G. Venanzoni [Fermilab E989 Collaboration], J. Phys. Conf. Ser. **349**, 012008 (2012). (E989 experiment at Fermilab: <http://gm2.fnal.gov/>)
9. N. Saito [J-PARC g-2/EDM Collaboration], AIP Conf. Proc. **1467**, 45 (2012)

10. T. Aoyama, M. Hayakawa, T. Kinoshita, M. Nio, Phys. Rev. Lett. **109**, 111808 (2012)
11. A. Czarnecki, W.J. Marciano, A. Vainshtein, Phys. Rev. D **67**, 073006 (2003). [Erratum-ibid. D **73**, 119901 (2006)]
12. C. Gnendiger, D. Stockinger, H. Stockinger-Kim, Phys. Rev. D **88**, 053005 (2013)
13. K. Hagiwara, R. Liao, A.D. Martin, D. Nomura, T. Teubner, J. Phys. G **38**, 085003 (2011)
14. A. Kurz, T. Liu, P. Marquard, M. Steinhauser, Phys. Lett. B **734**, 144 (2014)
15. M. Davier, A. Hoecker, B. Malaescu, Z. Zhang, Eur. Phys. J. C **71**, 1515 (2011). [Erratum-ibid. C **72**, 1874 (2012)]
16. J. Prades, E. de Rafael, A. Vainshtein, Advanced Series on Directions in High Energy Physics, vol. 20. [arXiv:0901.0306](https://arxiv.org/abs/0901.0306) [hep-ph]
17. F.S. Queiroz, W. Shepherd, Phys. Rev. D **89**, 095024 (2014)
18. C. Bouchiat, L. Michel, J. Phys. Radium **22**, 121 (1961)
19. L. Durand, Phys. Rev. **128**, 441 (1962)
20. M. Gourdin, E. De Rafael, Nucl. Phys. B **10**, 667 (1969)
21. E. de Rafael, Phys. Lett. B **322**, 239 (1994)
22. M. Hayakawa, T. Kinoshita, A.I. Sanda, Phys. Rev. Lett. **75**, 790 (1995)
23. M. Hayakawa, T. Kinoshita, Phys. Rev. D **57**, 465 (1998). [Erratum-ibid. D **66**, 019902 (2002)]
24. M. Knecht, A. Nyffeler, Phys. Rev. D **65**, 073034 (2002)
25. K. Melnikov, A. Vainshtein, Phys. Rev. D **70**, 113006 (2004)
26. A. Nyffeler, Phys. Rev. D **79**, 073012 (2009)
27. K. Kampf, J. Novotny, Phys. Rev. D **84**, 014036 (2011)
28. P. Roig, A. Guevara, G.L. Castro, Phys. Rev. D **89**, 073016 (2014)
29. K.T. Engel, M.J. Ramsey-Musolf, Phys. Lett. B **738**, 123 (2014)
30. J. Bijnens, E. Pallante, J. Prades, Phys. Rev. Lett. **75**, 1447 (1995)
31. J. Bijnens, E. Pallante, J. Prades, Nucl. Phys. B **474**, 379 (1996)
32. J. Bijnens, E. Pallante, J. Prades, Nucl. Phys. B **626**, 410 (2002)
33. E. Bartos, A.Z. Dubnickova, S. Dubnicka, E.A. Kuraev, E. Zemlyanaya, Nucl. Phys. B **632**, 330 (2002)
34. A.A. Pivovarov, Phys. At. Nucl. **66**, 902 (2003). [Yad. Fiz. **66**, 934 (2003)]
35. J. Erler, G. Toledo Sanchez, Phys. Rev. Lett. **97**, 161801 (2006)
36. R. Boughezal, K. Melnikov, Phys. Lett. B **704**, 193 (2011)
37. D. Greynat, E. de Rafael, JHEP **1207**, 020 (2012)
38. A.E. Dorokhov, W. Broniowski, Eur. Phys. J. C **32**, 79 (2003)
39. A.E. Dorokhov, Phys. Rev. D **70**, 094011 (2004)
40. A.E. Dorokhov, Eur. Phys. J. C **42**, 309 (2005)
41. A.E. Dorokhov, Acta Phys. Pol. B **36**, 3751 (2005)
42. A.E. Dorokhov, W. Broniowski, Phys. Rev. D **78**, 073011 (2008)
43. A.E. Dorokhov, A.E. Radzhabov, A.S. Zhevlakov, Eur. Phys. J. C **71**, 1702 (2011)
44. A.E. Dorokhov, A.E. Radzhabov, A.S. Zhevlakov, Eur. Phys. J. C **72**, 2227 (2012)
45. T. Goecke, C.S. Fischer, R. Williams, Phys. Rev. D **83**, 094006 (2011). [Erratum-ibid. D **86**, 099901 (2012)]
46. T. Goecke, C.S. Fischer, R. Williams, Phys. Rev. D **87**, 034013 (2013)
47. D.K. Hong, D. Kim, Phys. Lett. B **680**, 480 (2009)
48. L. Cappiello, O. Cata, G. D'Ambrosio, Phys. Rev. D **83**, 093006 (2011)
49. G. Colangelo, M. Hoferichter, M. Procura, P. Stoffer, JHEP **1409**, 091 (2014)
50. V. Pauk, M. Vanderhaeghen, Phys. Rev. D **90**, 113012 (2014)
51. P. Masjuan, M. Vanderhaeghen. [arXiv:1212.0357](https://arxiv.org/abs/1212.0357) [hep-ph]
52. R. Escribano, P. Masjuan, P. Sanchez-Puertas, Phys. Rev. D **89**, 2378 (2014)
53. J. Aldins, T. Kinoshita, S.J. Brodsky, A.J. Dufner, Phys. Rev. D **1**, 034014 (1970)
54. E.A. Kuraev, Z.K. Silagadze, A.A. Chesel, A. Schiller, Sov. J. Nucl. Phys. **50** (1989) 264. [Yad. Fiz. **50** (1989) 422]
55. A.B. Arbuzov, V.V. Bytev, E.A. Kuraev, E. Tomasi-Gustafsson, Y.M. Bystritskiy, Phys. Part. Nucl. **42**, 79 (2011)
56. S. Mandelstam, Ann. Phys. **19**, 1 (1962)
57. J. Terning, Phys. Rev. D **44**, 887 (1991)
58. Y. Liao, Eur. Phys. J. C **60**, 125 (2009)
59. A.E. Dorokhov, M.K. Volkov, J. Hufner, S.P. Klevansky, P. Rehberg, Z. Phys. C **75**, 127 (1997)
60. A.A. Osipov, A.E. Radzhabov, M.K. Volkov, Phys. At. Nucl. **70**, 1931 (2007)
61. A. Scarpettini, D. Gomez Dumm, N.N. Scoccola, Phys. Rev. D **69**, 114018 (2004)